Polymer Testing 109 (2022) 107544

Contents lists available at ScienceDirect

Polymer Testing

journal homepage: www.elsevier.com/locate/polytest

# Effect of uncertainty on dynamic damping and stiffness of spherical hollow rubber isolators based on harmonic experiment

Hao Li [a,b], Chengliang Yang [a,*], Shaoxin Wang [a], Ping Su [a], Xingyun Zhang [a], Zenghui Peng [a], Quanquan Mu [a]

[a] State Key Laboratory of Applied Optics, Changchun Institute of Optics, Fine Mechanics and Physics, Chinese Academy of Sciences, Changchun, 130033, China
[b] Center of Materials Science and Optoelectronics Engineering, University of Chinese Academy of Sciences, Beijing, 100049, China

ARTICLE INFO

*Keywords:*
Spherical rubber isolator
Dynamic stiffness
Dynamic damping
Uncertain parameters
Resonant frequency

ABSTRACT

This study aims to identify the effect of uncertainty on the dynamic characteristics of a thin-walled hollow spherical rubber isolator. Firstly, the nonlinearity and uncertainties of the spherical rubber isolator were obtained by swept-sine experiments. The relationship between dynamic stiffness and damping against relative displacement amplitude was established. Then, a high-order polynomial function with uncertain parameters introduced was used for simulation. The uncertain parameters were quantified using the singular value decomposition and Monte Carlo simulations. Furthermore, the dynamic stiffness and damping of the experimental data were optimized using the Covariance Matrix Adaptation and Evolution Strategy. Finally, the high consistency between the simulation results and experimental results were demonstrated. Overall, the nonlinear model established according to the uncertain parameter quantization is feasible. This method can predict the nonlinear characteristics of the rubber isolator well and also may be applied to other nonlinear models.

## 1. Introduction

In recent years, viscoelastic materials such as rubber materials are used in a wide range of engineering fields (space applications, actuators, sensors, etc) due to their relative softness, the capability to withstand excessive deformation, and restoration of their original shape after stress release. Notably, rubber isolators play an irreplaceable role in some special occasions where non-magnetic requirements are needed. However, the complexity of manufactured rubber isolators is exacerbated due to their significant frequency dependence and nonlinear dynamic behavior when excited [1]. The dynamic behaviors of rubber isolators refer to dynamic stiffness and damping, which mainly depend on the chemical compositions in the rubber material, vibration frequency, vibration amplitude, temperature and humidity [2–4]. Component nonlinearities are attributed to material properties or geometric influences [5]. Nevertheless, studies on the nonlinear dynamic behavior of rubber materials are relatively limited, especially for thin-walled hollow spherical rubber isolators. In order to improve the vibration performance of spherical rubber isolators and serve the structure design better, studies of the characteristics of spherical rubber isolators are needed.

Numerous methods [6–8] have been established to demonstrate the dynamic behavior of rubber isolators. For example, methods based on the modeling of the mechanical laws of the elastomer use physical models such as the Kelvin-Voigt or Maxwell model, fractional derivatives or the Berg model. These methods give accurate outputs but require extremely complex structural modeling, generally using a finite element [9] discretization of the joint element. Efforts have also been devoted to experimentally based phenomenological modeling. Chen X. Q. and Sun D.W. et al. used polynomial or exponential function to fit the dependence of the dynamic stiffness and damping on the relative amplitude [10,11]. Roncen T. et al. performed experiments and numerical simulations of a nonlinear rubber isolator using the Harmonic Balance Method and the shooting method [12]. Good correlations for harmonic and broadband random excitations were observed [12].

This study aims to use phenomenological modeling with experimental and analytical approaches to explore the nonlinear behavior of a thin-walled hollow spherical rubber isolator subjected to harmonic excitation and to interpret the effect of uncertainty on the dynamic characteristics. This paper is presented in the following sections. In Section 2, the experimental setup of the harmonic experiment is presented and the results of the experiment are analyzed. In Section 3, the nonlinear modeling and nonlinear dynamic parameters identification are discussed. In Section 4, the simulations of uncertain parameters are

* Corresponding author. Changchun Institute of Optics, Fine Mechanics and Physics, Chinese Academy of Sciences, Changchun, China.
*E-mail address:* chengliangyang@ciomp.ac.cn (C. Yang).

https://doi.org/10.1016/j.polymertesting.2022.107544
Received 6 April 2021; Received in revised form 28 February 2022; Accepted 10 March 2022
Available online 18 March 2022
0142-9418/

**Abbreviations**

| | |
|---|---|
| $K$ | stiffness |
| $C$ | damping |
| $f$ | resonant frequency |
| $Q$ | maximum FRF amplitude |
| $\omega_{\max}$ | associated angular frequency |
| $\xi$ | damping ratio |
| $\omega_0$ | natural frequency |
| $q$ | displacement amplitude of the base excitation |
| M | mass |
| $X$ | relative displacement of the mass M |
| $K_{\text{non}-lin}$ | nonlinear stiffness |
| $C_{\text{non}-lin}$ | nonlinear damping |
| $\alpha_i, i = 1, 2, 3, 4, 5$ | stiffness coefficients |
| $\beta_i, i = 1, 2, 3, 4, 5$ | damping coefficients |
| $\omega$ | frequency of the exciting force |
| $k_{es}$ | equivalent stiffness |
| $c_{ed}$ | equivalent damping |
| S | sample matrix |
| U | orthogonal matrix |
| $\Sigma$ | diagonal matrix |
| V | column vector |

validated by comparison with the experimental results. Conclusions are presented in Section 5.

## 2. Experiments

In order to investigate the vibration characteristics of a thin-walled hollow spherical rubber isolator, swept-sine experiments based on different acceleration excitations were performed.

### 2.1. Experimental setup

Fig. 1 shows the structure and the geometric parameters of the spherical rubber isolator. The vibration system consists of an electromagnetic shaker, vibration tooling, rubber isolator, mass block and accelerometers (Fig. 2). The linear bearing and guide shaft were used to suppress the vibration mode of the isolator in other directions; thereby the main vibration of the isolator was along X-direction. Meanwhile, two accelerometers were positioned symmetrically at 180° from each other at the bottom of the mass block with acceleration levels averaged to minimize the potential tilting.

The total mass of the experimental load was 50 grams with the mass of accelerometers A2 and A3 taken into account in the calculations. The acceleration levels of the input excitation were [0.3; 0.35; 0.4; 0.45; 0.5; 0.55; 0.6; 0.65; 0.7; 0.8; 0.9; 1.0; 1.1; 1.2; 1.3; 1.4; 1.5; 1.6] $g$. The swept-sine experiment for each acceleration level was repeated 10 times over the frequency range [30; 250] Hz at room temperature. The response was considered as stationary since the frequency evolved slowly (0.5 octave/min).

### 2.2. Experimental results

The frequency response functions (FRF) for different acceleration excitation levels were obtained in the swept-sine experiments, where each FRF curve was randomly selected from 10 experimental measurements (Fig. 3). As the acceleration level increased, resonance frequency reduced from 240 Hz to 50 Hz. The maximum FRF amplitude increased significantly at acceleration excitation of 1.5 $g$ and 1.6 $g$. The results indicate the significant nonlinear effect of the rubber isolator subjected to harmonic vibrations.

Table 1 plots the results of the resonant frequency $f$ and maximum FRF amplitude $Q$ for 10 experimental measurements with acceleration excitation levels of [0.4; 0.7; 1.0; 1.3; 1.6] $g$. Our findings show that under the same acceleration excitation level, the FRF varied in each experimental measurement, indicating the existence of uncertainty in the dynamic stiffness and damping of the rubber isolator when subjected to harmonic vibrations. Therefore, the errors caused by the uncertainty of dynamic stiffness and dynamic damping should be introduced into the nonlinear equations for the accuracy of nonlinear modeling.

### 2.3. Dynamic parameters modeling

To study the nonlinear characteristics of the spherical rubber isolator, the dynamic stiffness and damping were calculated using FRF. Based on the phenomenological modeling, we established the relationship between dynamic stiffness and dynamic damping versus relative displacement amplitude, and then introduced the uncertain parameters of the vibration system into the nonlinear modeling to improve its accuracy.

The dynamic parameters were calculated as follows. The FRF for a given acceleration excitation was obtained from the harmonic experiment. Then the maximum FRF amplitude $Q$ and associated angular frequency $\omega_{\max}$ were determined, and the damping ratio $\xi$ was calculated by $Q \approx 1/2\xi$. The natural frequency $\omega_0$ was calculated by $\omega_0 = \omega_{\max}/\sqrt{1-2\xi^2}$. Through the formula $\omega_0 = \sqrt{K/M}$ and $\xi = C/2M\omega_0$, the damping and stiffness under a given acceleration excitation were obtained. Fig. 4 shows the relationship between dynamic stiffness and

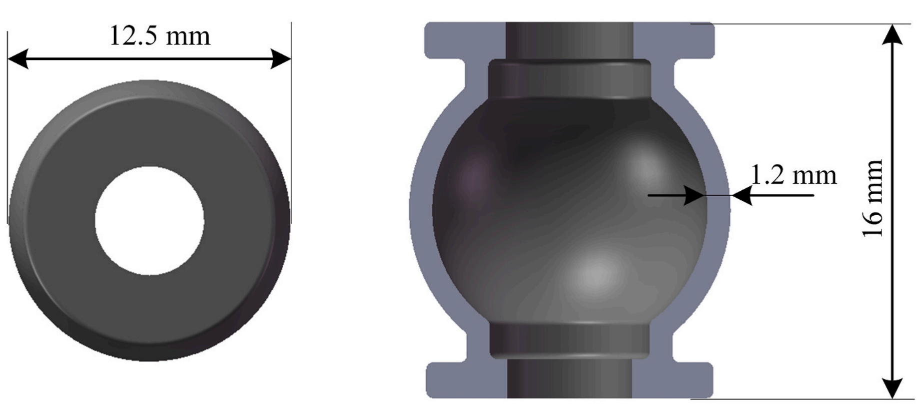


**Fig. 1.** A schematic of the spherical rubber isolator structure.

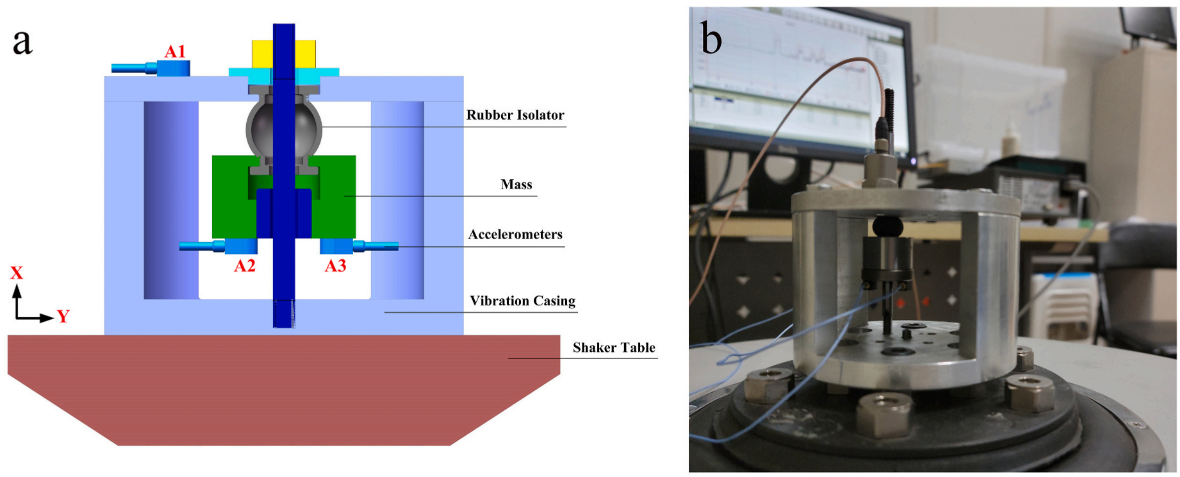


**Fig. 2.** (a) Structure of the experimental setup and sensor position. A1 is the accelerometer for the control signal, A2 and A3 are the output accelerometers. (b) Photograph of the experimental system.

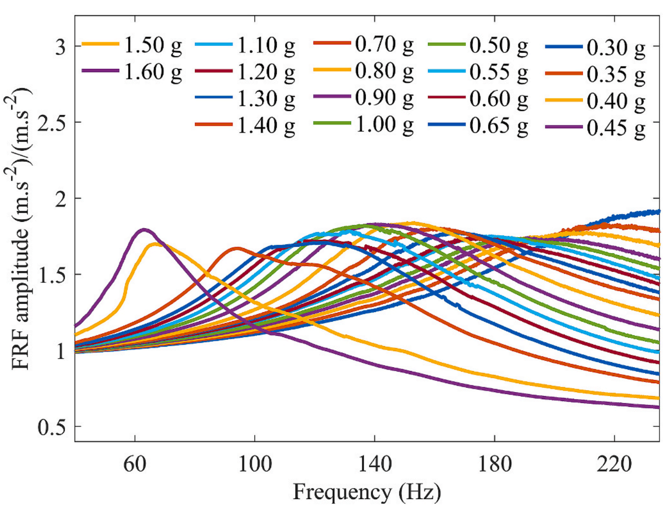


**Fig. 3.** FRF of swept-sine experiments at different excitation levels.

dynamic damping versus relative displacement amplitude. A decrease in the stiffness and damping could be observed when the displacement amplitude increased, providing additional evidence of the nonlinear effect of the spherical rubber isolator.

## 3. Nonlinear modeling

In order to investigate the effect of uncertainty on the dynamic characteristics of the spherical rubber isolator, the uncertainty needs to be analyzed and further quantified by introducing the parameters introduced into the nonlinear model. Multiple modeling methods for nonlinear models were proposed to predict the vibration characteristics and uncertainty of the isolation systems. For example, Chen X.Q. et al. [10] introduced the 2nd-order polynomial function to illuminate the effect of excitation amplitude on nonlinear characteristics, which brought out reliable simulation results. However, considering the dynamic stiffness and damping of the spherical rubber isolator, the 2nd-order polynomial function is no longer able to fit the nonlinear model accurately. In this regard, the 4th-order polynomial function was used for the spherical rubber isolator with the experimental uncertainty introduced into the nonlinear model. Based on this approach, we simplified the vibration system to a single-degree-of-freedom system (Fig. 5) consisting of nonlinear stiffness $K_{\text{non}-lin}$, nonlinear damping $C_{\text{non}-lin}$ and mass M. The dynamic differential equation of the vibration system could be written as follows,

$$\mathrm{M}\ddot{\mathrm{X}}(\mathrm{t}) + C_{\text{non}-lin}\dot{X}(\mathrm{t}) + K_{\text{non}-lin}X(\mathrm{t}) = -M\ddot{q}(\mathrm{t}) \tag{1}$$

where, $q$ is the displacement amplitude of the base excitation, and $X$ corresponds to the relative displacement of the mass M.

The 4th-order polynomial functions were fitted to $C_{\text{non}-lin}$、 $K_{\text{non}-lin}$, and the equations were written in the following form,

$$C_{\text{non}-lin} = \beta_1 + \beta_2|\mathrm{X}| + \beta_3\mathrm{X}^2 + \beta_4|\mathrm{X}|^3 + \beta_5\mathrm{X}^4 \tag{2}$$

$$K_{\text{non}-lin} = \alpha_1 + \alpha_2|\mathrm{X}| + \alpha_3\mathrm{X}^2 + \alpha_4|\mathrm{X}|^3 + \alpha_5\mathrm{X}^4 \tag{3}$$

where, $\beta_i, i = 1, 2, 3, 4, 5$ represents the damping coefficients and $\alpha_i, i =$

**Table 1**
Results of resonant frequencies and maximum FRF amplitudes.

| Excitation | | Case 1 | Case 2 | Case 3 | Case 4 | Case 5 | Case 6 | Case 7 | Case 8 | Case 9 | Case 10 |
|---|---|---|---|---|---|---|---|---|---|---|---|
| 0.4 *g* | *f* (Hz) | 228.34 | 222.62 | 218.96 | 218.99 | 212.97 | 211.08 | 210.32 | 210.14 | 211.45 | 213.16 |
| | *Q* | 1.972 | 1.973 | 1.855 | 1.861 | 1.862 | 1.880 | 1.875 | 1.878 | 1.863 | 1.856 |
| 0.7 *g* | *f* (Hz) | 183.22 | 182.22 | 189.41 | 187.89 | 195.41 | 197.14 | 200.49 | 198.08 | 191.28 | 192.66 |
| | *Q* | 1.758 | 1.750 | 1.748 | 1.743 | 1.744 | 1.750 | 1.748 | 1.742 | 1.742 | 1.744 |
| 1.0 *g* | *f* (Hz) | 114.57 | 119.23 | 117.85 | 125.64 | 118.60 | 120.59 | 112.38 | 117.85 | 123.17 | 110.91 |
| | *Q* | 1.534 | 1.513 | 1.522 | 1.525 | 1.518 | 1.511 | 1.507 | 1.503 | 1.506 | 1.502 |
| 1.3 *g* | *f* (Hz) | 87.29 | 81.38 | 99.66 | 94.30 | 91.39 | 85.06 | 92.71 | 94.05 | 89.13 | 97.55 |
| | *Q* | 1.492 | 1.475 | 1.479 | 1.465 | 1.447 | 1.466 | 1.442 | 1.444 | 1.432 | 1.436 |
| 1.6 *g* | *f* (Hz) | 75.30 | 68.38 | 65.55 | 67.53 | 70.11 | 63.44 | 69.05 | 76.99 | 68.98 | 64.87 |
| | *Q* | 2.137 | 1.928 | 1.887 | 1.991 | 2.013 | 2.095 | 2.088 | 2.110 | 2.120 | 2.105 |

*f*, resonant frequency; *Q*, maximum FRF amplitude.

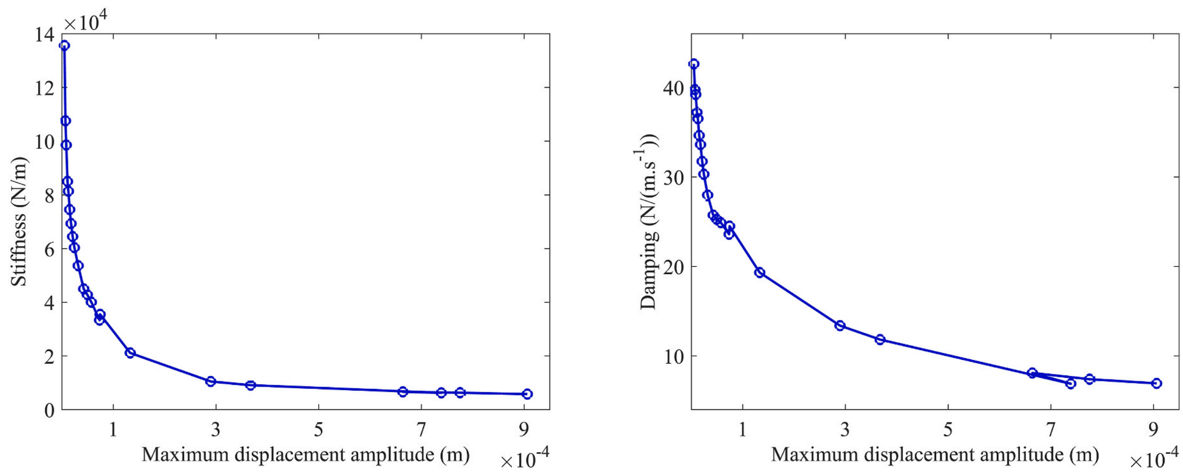


**Fig. 4.** Evolution of the dynamic stiffness (a) and the dynamic damping (b) with respect to the displacement amplitude.

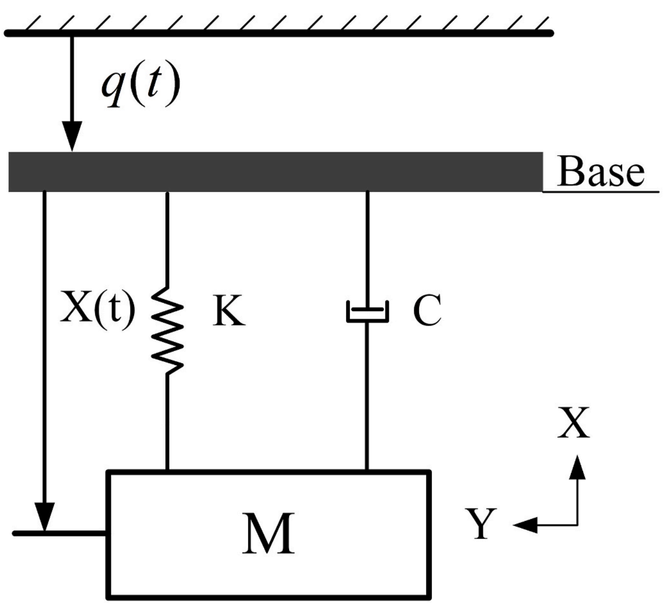


**Fig. 5.** Diagram of the rubber isolator modeled by a single-degree-of-freedom system.

1, 2, 3, 4, 5 represents the stiffness coefficients. To obtain a standard dynamic equation, bilateral sides of the original dynamic differential equation were divided by mass M.

We simplified the general nonlinear motion equation by ignoring the exciting force in the following form.

$$\ddot{X}(t) + \omega_0^2 X = f(X, \dot{X}) \tag{4}$$

$$\begin{aligned} f(X, \dot{X}) = & -\left(\beta_1 + \beta_2|X| + \beta_3 X^2 + \beta_4|X|^3 + \beta_5 X^4\right)\dot{X} - \\ & \left(\alpha_1 + \alpha_2|X| + \alpha_3 X^2 + \alpha_4|X|^3 + \alpha_5 X^4\right)X + \omega_0^2 X \end{aligned} \tag{5}$$

$\omega_0$ represents the natural frequency of the linear system. The 1st-order approximate solution of the equation was written as follows according to reference [13].

$$X = A\cos\varphi \tag{6}$$

$$\dot{X} = -A\omega_0 \sin\varphi \tag{7}$$

The equivalent stiffness $k_{es}$ and equivalent damping $c_{ed}$ were defined as follows

$$k_{es} = \omega_0^2 - \frac{1}{\pi A}\int_0^{2\pi} f(X, \dot{X})\cos\varphi d\varphi \tag{8}$$

$$c_{ed} = \frac{1}{\pi A \omega_0}\int_0^{2\pi} f(X, \dot{X})\sin\varphi d\varphi \tag{9}$$

Substituting equations (6) and (7) into (8) and (9), we obtained the following equation after simplification.

$$k_{es} = \alpha_1 + \frac{8A}{3\pi}\alpha_2 + \frac{3A^2}{4}\alpha_3 + \frac{32A^3}{15\pi}\alpha_4 + \frac{5A^4}{8}\alpha_5 \tag{10}$$

$$c_{ed} = \beta_1 + \frac{4A}{3\pi}\beta_2 + \frac{A^2}{4}\beta_3 + \frac{8A^3}{15\pi}\beta_4 + \frac{A^4}{8}\beta_5 \tag{11}$$

The motion differential equation of system can be written in the following form,

$$\ddot{x} + 2\varsigma\omega_n\dot{x} + \omega_n^2 x = q\omega^2 \sin\omega t \tag{12}$$

where , $\omega_n = \sqrt{k_{es}}$, $2\varsigma\omega_n = c_{ed}$, $\omega$ is the frequency of the exciting force, and $q$ is the displacement amplitude of the base excitation. Because the excitation is a harmonic function, the stationary response can be seen as a harmonic function with the same frequency. Therefore, the solution of equation (12) can be written as follows,

$$x = A\sin(\omega t - \varphi) \tag{13}$$

where

$$A = \frac{q}{\sqrt{(k_{es} - \omega^2)^2 + (c_{ed}\omega)^2}} \tag{14}$$

$$\tan\varphi = \frac{c_{ed}\omega}{k_{ed} - \omega^2} \tag{15}$$

When $\omega_n^2 \approx \omega^2$, the function amplitude has a maximum value $A_{\max}$. Therefore, the following equations can be obtained by combining Equation (10)–(11)

$$\omega_n^2 = \alpha_1 + \frac{8A_{\max}}{3\pi}\alpha_2 + \frac{3A_{\max}{}^2}{4}\alpha_3 + \frac{32A_{\max}{}^3}{15\pi}\alpha_4 + \frac{5A_{\max}{}^4}{8}\alpha_5 \tag{16}$$

$$2\varsigma\omega_n = \beta_1 + \frac{4A_{\max}}{3\pi}\beta_2 + \frac{A_{\max}{}^2}{4}\beta_3 + \frac{8A_{\max}{}^3}{15\pi}\beta_4 + \frac{A_{\max}{}^4}{8}\beta_5 \tag{17}$$

Based on a series of experimental results of the swept-sine experiments, the polynomial coefficients of dynamic stiffness and damping can be calculated by combining Equations (16) and (17) (as shown in Table 2). The coefficients varied in different experimental measurements, indicating the uncertainty of the vibration characteristics of the spherical rubber isolator when subjected to harmonic excitation. Therefore, in order to clarify the effect of the uncertainty on the dynamic characteristics of the rubber isolator, the uncertain parameters should to be further quantified.

## 4. Simulation

We introduced the uncertain parameters into the nonlinear model using a 4th-order polynomial function. The effects of the uncertain parameters on the nonlinear dynamic characteristics of the spherical rubber isolator were investigated, including resonant frequency, dynamic stiffness and damping.

### 4.1. Quantification and analysis of uncertain parameters

We quantified the uncertainty of the dynamic stiffness and damping using polynomial coefficients as follows (Fig. 6). Firstly, correlation analysis between the polynomial coefficients was performed, which is a prerequisite for principal component analysis. $p < 0.05$ is considered statistically significant. The bartlett's sphericity test showed a significant correlation between the polynomial coefficients ($p = 8.37E\text{-}5$). Then, the coefficients with correlations were transformed into mutually independent coefficients. A sample matrix S was constructed using the raw data of the polynomial coefficients. Then principal component analysis was performed to remove the correlation by analyzing the sample matrix with the application of the Singular Value Decomposition (SVD) [14,15],

$$S' = U\sum V^T \tag{18}$$

where , S is the sample matrix, U is the orthogonal matrix, $\sum$ is the diagonal matrix, and the column vector of V is the principal component of the sample matrix S.

Assuming that the principal component is a normal random variable, the principal component was resampled using the Monte Carlo algorithm (MC). The new sample matrix obtained after the inverse transformation were used as MC data for the following analysis. In order to verify the reliability of the MC data, a consistency analysis of the original data and the MC resample data was performed. Table 3 shows the mean deviations and variance deviations of the original data and MC data. The maximum deviations were 1.12% and 3.79%, respectively, indicating that the original data were in line with MC resample data. This further confirms the credibility of the MC samples for the following study.

Table 4 shows the values of the polynomial coefficients calculated by the probability method. The resonant frequency for different acceleration excitations were calculated using the data in Table 4 combined with Equation (16) (17) (Table 5). The deviations from the average resonant frequency values obtained from experimental measurements were also presented. Notably, the average deviation was less than 5%, suggesting that the nonlinear modeling and the quantification of the uncertain parameters can describe the characteristics of the vibration system very well.

### 4.2. Effect of uncertain parameters on resonance frequency

By introducing the uncertain parameters into the motion differential equation, the resonant frequency was obtained. Because the Cumulative Distribution Function (CDF) can describe the probability distribution of a random variable and simultaneously quantify the uncertain parameters in an intuitive manner, we calculated the CDF of uncertain parameters both from the simulation results and experimental results (Fig. 7). Black and green indicate the interval of experiments and 95% confidence interval of simulation, respectively. The results show that the CDF curves of the resonant frequency simulation results (red) were coincident with those of the experimental results (blue). Meanwhile, the resonant frequency decreased with the increase of acceleration excitation, which provides additional evidence for the softening effect of dynamic stiffness. However, for the higher excitation levels, the correlation of the resonant frequency between the simulation results and the experimental results were relatively weak, mainly owing to the heating of the elastomeric compound caused by high excitations.

### 4.3. Effect of uncertain parameters on dynamic characteristics

In order to investigate the effect of uncertain parameters on dynamic stiffness and damping, we transformed the motion equation (12) by setting experimental results of displacement amplitude as solutions of the equation to obtain the values of dynamic stiffness, dynamic damping and phase. In consideration of the nonlinear correlation between the stiffness and damping versus displacement amplitude, the equation was established as a nonlinear function and optimally solved by the Covariance Matrix Adaptation and Evolution Strategy (CMA-ES) algorithm, which is an evolutionary algorithm equipped with quick convergence and low noise sensitivity [16]. The CMA-ES algorithm guides the evolution path of the population through the dynamic step-size σ and the dynamic positive definite covariance matrix C. It is mainly used for real-parameter (continuous domain) optimization of nonlinear and non-convex functions. The basic equation is as follows,

$$x_k^{(g+1)} \sim m^{(g)} + \sigma^{(g)} N\left(0, C^{(g)}\right) \tag{19}$$

where , $N(0, C^{(g)})$ represents a multivariate normal distribution with zero mean and covariance matrix $C^{(g)}$; $x_k^{(g+1)}$ is the k-th offspring from the (g+1)-th generation; $m^{(g)}$ is the mean of the g-generation search distribution; $\sigma^{(g)}$ is the g-generation search step; $C^{(g)}$ is the covariance matrix of the g-generation; the iterative updating step is completed for calculation, including $m^{(g)}$ , $\sigma^{(g)}$ , $C^{(g)}$ updating process.

The dynamic stiffness, dynamic damping, and phase were set as variables and optimized using CMA-ES. The objective function was constructed with the variables introduced into the motion equation, and the range of the variables was used as a constraint to the optimization process. The variables ranged from the minimum values to the

**Table 2**
Polynomial coefficients of dynamic stiffness and damping.

| Coeff | Case 1 | Case 2 | Case 3 | Case 4 | Case 5 | Case 6 | Case 7 | Case 8 | Case 9 | Case 10 |
|---|---|---|---|---|---|---|---|---|---|---|
| $\alpha_1$ | 1.392E5 | 1.403E5 | 1.275E5 | 1.265E5 | 1.258E5 | 1.208E5 | 1.206E5 | 1.226E5 | 1.217E5 | 1.235E5 |
| $\alpha_2$ | −3.694E9 | −3.611E9 | −3.221E9 | −3.136E9 | −3.078E9 | −2.811E9 | −2.821E9 | −2.891E9 | −2.918E9 | −2.986E9 |
| $\alpha_3$ | 3.156E13 | 2.878E13 | 2.824E13 | 2.636E13 | 2.548E13 | 2.217E13 | 2.277E13 | 2.354E13 | 2.421E13 | 2.478E13 |
| $\alpha_4$ | −2.607E16 | −2.392E16 | −2.588E16 | −2.193E16 | −2.179E16 | −1.768E16 | −1.858E16 | −1.916E16 | −1.981E16 | −2.032E16 |
| $\alpha_5$ | −1.021E14 | −9.309E13 | −9.073E13 | −8.481E13 | −8.156E13 | −7.060E13 | −7.259E13 | −7.488E13 | −7.724E13 | −7.908E13 |
| $\beta_1$ | 4.245E1 | 4.259E1 | 4.286E1 | 4.268E1 | 4.248E1 | 4.111E1 | 4.131E1 | 4.169E1 | 4.166E1 | 4.204E1 |
| $\beta_2$ | −4.736E5 | −4.506E5 | −4.902E5 | −4.822E5 | −4.613E5 | −3.881E5 | −4.085E5 | −4.068E5 | −4.226E5 | −4.297E5 |
| $\beta_3$ | 3.380E9 | 2.832E9 | 3.631E9 | 3.464E9 | 3.212E9 | 2.348E9 | 2.690E9 | 2.628E9 | 2.906E9 | 2.921E9 |
| $\beta_4$ | −2.718E12 | −2.211E12 | −3.240E12 | −2.816E12 | −2.679E12 | −1.759E12 | −2.127E12 | −2.047E12 | −2.321E12 | −2.321E12 |
| $\beta_5$ | −1.065E10 | −8.604E9 | −1.136E10 | −1.089E10 | −1.003E10 | −7.027E09 | −8.308E09 | −7.999E09 | −9.048E09 | −9.034E09 |

Coeff, coefficients.

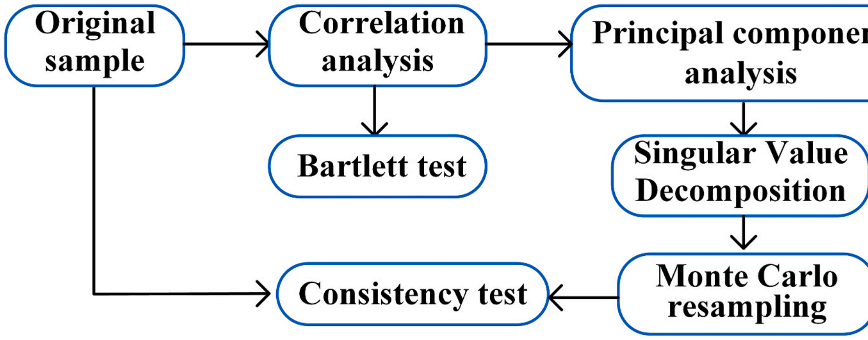


**Fig. 6.** A schematic of uncertainty quantification algorithms.

**Table 3**
Mean and variance deviations of the original data and MC data.

| Coeff | $\alpha_1$ | $\alpha_2$ | $\alpha_3$ | $\alpha_4$ | $\alpha_5$ | $\beta_1$ | $\beta_2$ | $\beta_3$ | $\beta_4$ | $\beta_5$ |
|---|---|---|---|---|---|---|---|---|---|---|
| Mean deviation (%) | 0.81 | 0.61 | 0.42 | 0.59 | 0.15 | 0.22 | 0.72 | 0.47 | 1.12 | 0.18 |
| Variance deviation (%) | 1.73 | 0.91 | 1.31 | 2.32 | 2.35 | 2.26 | 3.79 | 2.08 | 2.71 | 2.58 |

Coeff, coefficients; MC, Monte Carlo algorithm.

**Table 4**
Values of the polynomial coefficients.

| Coeff | $\alpha_1$ | $\alpha_2$ | $\alpha_3$ | $\alpha_4$ | $\alpha_5$ | $\beta_1$ | $\beta_2$ | $\beta_3$ | $\beta_4$ | $\beta_5$ |
|---|---|---|---|---|---|---|---|---|---|---|
| | 1.283E5 | −3.215E9 | 2.840E13 | −2.59E16 | −9.255E13 | 4.209E1 | −4.418E5 | 3.016E9 | −2.451E12 | −9.278E9 |

Coeff, coefficients.

**Table 5**
Resonant frequency at different acceleration excitation levels.

| Excitation ($g$) | 0.3 | 0.35 | 0.4 | 0.45 | 0.5 | 0.55 | 0.6 | 0.65 | 0.7 |
|---|---|---|---|---|---|---|---|---|---|
| $f$ (Hz) | 235.34 | 210.67 | 207.69 | 197.55 | 193.70 | 183.94 | 176.32 | 173.93 | 168.65 |
| Deviation (%) | 2.97 | 2.85 | 1.45 | 3.05 | 2.59 | 2.19 | 1.70 | 3.46 | 4.17 |
| Excitation ($g$) | 0.8 | 0.9 | 1.0 | 1.1 | 1.2 | 1.3 | 1.4 | 1.5 | 1.6 |
| $f$ (Hz) | 153.03 | 135.45 | 128.46 | 124.49 | 120.87 | 115.84 | 100.33 | 71.29 | 68.28 |
| Deviation (%) | 0.65 | 3.70 | 6.25 | 5.64 | 1.67 | 4.95 | 5.87 | 3.04 | 4.35 |

$f$, resonant frequency.

maximum values of the experimental results of dynamic stiffness and damping. Fig. 8 shows the results of the stiffness and damping optimization calculated by the CMA-ES algorithm at an excitation level of 0.4 $g$ (indicated as triangles) and the dynamic stiffness and damping distributions calculated using the MC resampling data combined with Equation (16)(17) (indicated as lines). It can be noted that the results of nonlinear stiffness and damping optimized by CMA-ES were in the range of the calculation based on the uncertain parameters. Therefore, our results demonstrate that the nonlinear modeling with uncertainty introduced are feasible to predict the dynamic characteristics (dynamic stiffness and damping) of the spherical rubber isolator.

## 5. Conclusions

In this work, the effects of uncertainty on dynamic damping and stiffness of spherical rubber isolators were studied based on swept-sine experiments at different acceleration excitation levels. A nonlinear model of the dynamic characteristics of spherical rubber isolators was established by using a 4th-order polynomial function with the uncertain parameters introduced. The uncertainty of the coefficients was quantified by combining SVD with MC algorithms. The dynamic stiffness and damping of the experimental data were further optimized using the CMA-ES algorithm. The calculated frequency, dynamic stiffness and damping agreed with the experimental results. In conclusion, the approach of nonlinear model with the uncertain parameter quantization is able to predict the dynamic characteristics of the spherical rubber isolator. The uncertainty is also proved to be very important for the spherical rubber isolation systems. The proposed simulation approach may facilitate the practical applications of the isolation system.

## Funding

National Natural Science Foundation of China (11774342 and 61805238), the Foundation of State Key Laboratory of Applied Optics.

## Author statement

Hao Li: Investigation, Methodology, Visualization, Writing - review & editing. Chengliang Yang: Supervision, Writing - review & editing. Shaoxin Wang: Methodology. Ping Su: Resources. Xingyun Zhang: Data Curation. Zenghui Peng: Supervision. Quanquan Mu: Validation.

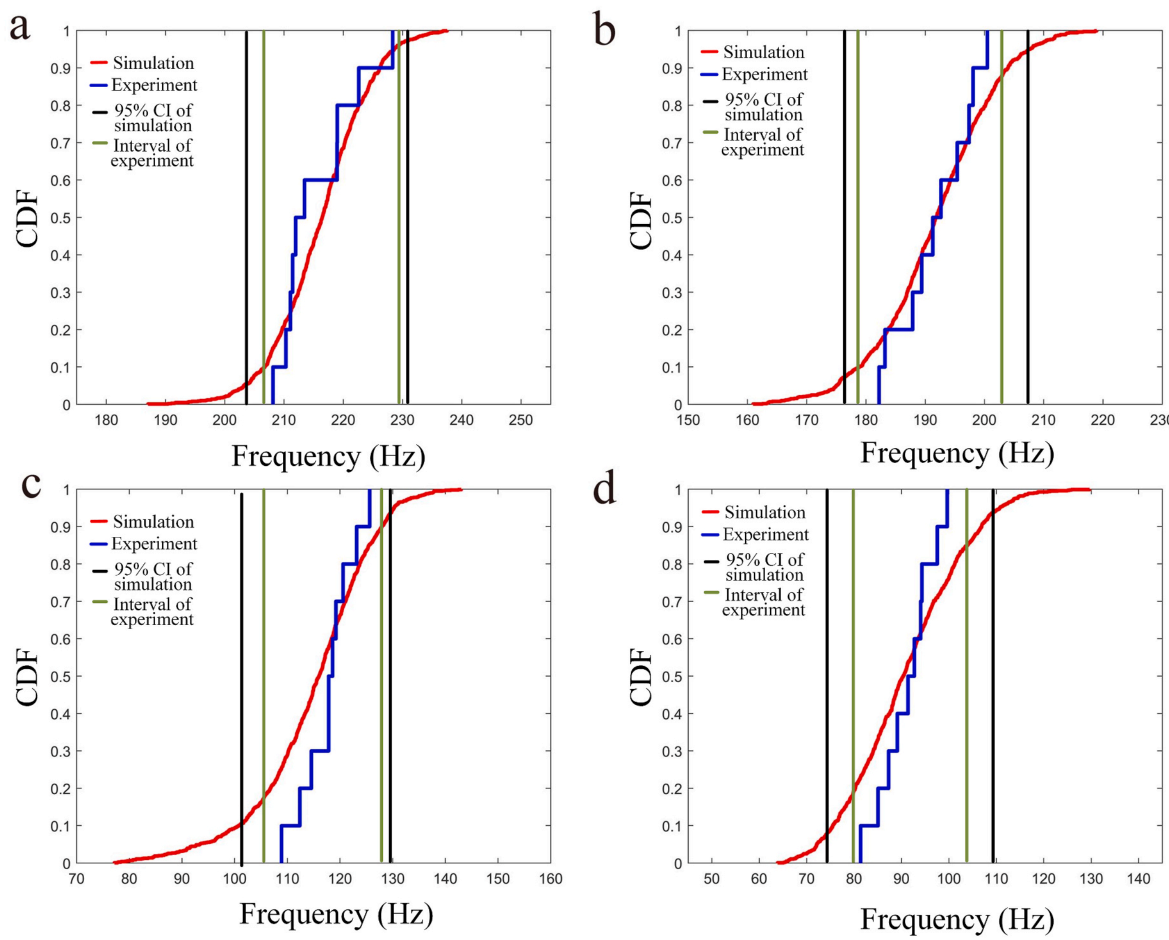


**Fig. 7.** Comparison of the resonant frequency between the simulation results and the experimental results. (a) vibration level of 0.4 *g*; (b) vibration level of 0.7 *g*; (c) vibration level of 1 *g*; (d) vibration level of 1.3 *g*. CDF, Cumulative Distribution Function.

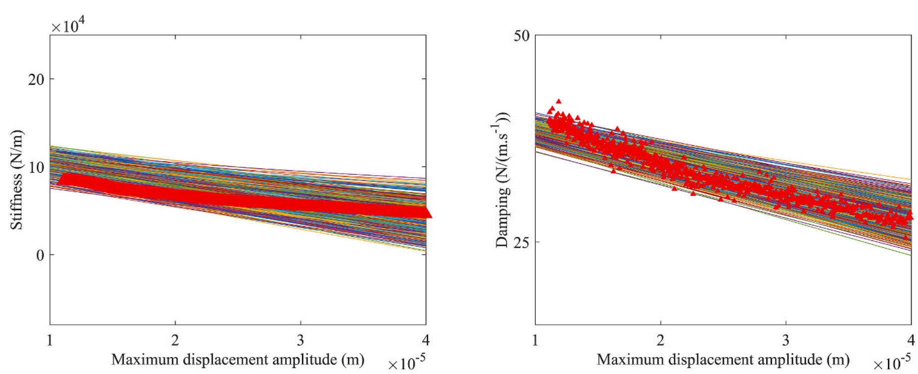


**Fig. 8.** Comparison of the dynamic stiffness (a) and damping (b) between the simulation results and the experimental results at vibration level of 0.4 *g*.

## Data availability

The datasets used and/or analyzed during the current study are available from the corresponding author on reasonable request.

## Declaration of competing interest

The authors declare that they have no known competing financial interests or personal relationships that could have appeared to influence the work reported in this paper.

## Acknowledgments

This work was supported by CAS Interdisciplinary Innovation Team and Youth Innovation Promotion Association CAS.

## References

[1] K.D. Papoulia, J.M. Kelly, Visco-hyperelastic model for filled rubbers used in vibration isolation, J. Eng. Mater. Technol. 119 (1997) 292–297.
[2] M. Sjöberg, L. Kari, Testing of nonlinear interaction effects of sinusoidal and noise excitation on rubber isolator stiffness, Polym. Test. 22 (2003) 343–351.

[3] C.M. Richards, R. Singh, Characterization of rubber isolator nonlinearities in the context of single- and multi-degree-of-freedom experimental systems, J. Sound Vib. 247 (2001) 807–834.
[4] D. Ponnamma, K.K. Sadasivuni, M. Strankowski, P. Moldenaers, S. Thomas, Y. Grohens, Interrelated shape memory and Payne effect in polyurethane/graphene oxide nanocomposites, RSC Adv. 3 (2013).
[5] J. Harris, A. Stevenson, On the role of nonlinearity in the dynamic behaviour of rubber components, Rubber Chem. Technol. 59 (5) (1986) 740–764.
[6] R. Lewandowski, B. Chorążyczewski, Identification of the parameters of the Kelvin–Voigt and the Maxwell fractional models, used to modeling of viscoelastic dampers, Comput. Struct. 88 (2010) 1–17.
[7] M.M. Sjberg, L. Kari, Non-linear behavior of a rubber isolator system using fractional derivatives, Veh. Syst. Dyn. 37 (2002) 217–236.
[8] M. Berg, A non-linear rubber spring model for rail vehicle dynamics analysis, Veh. Syst. Dyn. 30 (1998) 197–212.
[9] N. Gil-Negrete, J. Viñolas, L. Kari, A simplified methodology to predict the dynamic stiffness of carbon-black filled rubber isolators using a finite element code, J. Sound Vib. 296 (2006) 757–776.
[10] C. Xueqian, S. Zhanpeng, H. Qinshu, D. Qiang, L. Xin'en, Influence of uncertainty and excitation amplitude on the vibration characteristics of rubber isolators, J. Sound Vib. 377 (2016) 216–225.
[11] D.W. Sun, Z.G. Chen, G.Y. Zhang, P. Eberhard, Modeling and parameter identification of amplitude- and frequency-dependent rubber isolator, J. Cent. South Univ. Technol 18 (2011) 672–678.
[12] T. Roncen, J.J. Sinou, J.P. Lambelin, Experiments and nonlinear simulations of a rubber isolator subjected to harmonic and random vibrations, J. Sound Vib. 451 (2019) 71–83.
[13] R.E. Mickens, Oscillations in Planar Dynamic Systems, World Scientific, Singapore, 1996.
[14] T. Lyche, The Singular Value Decomposition, Numerical Linear Algebra and Matrix Factorizations, 2020.
[15] X. Wang, Z. Song, Y. Wang, Variational Quantum Singular Value Decomposition, 2020.
[16] Z. Bouzarkouna, D.Y. Ding, A. Auger, Method for Selecting Positions of Wells to Be Drilled for Exploiting an Oil Field, 2013.